Acoustic Backscatter: Enabling Ultra-Low Power, Precise Indoor Positioning.

Bert Cox
KU Leuven
DRAMCO Research Group
Ghent, Belgium
name.surname@kuleuven.be

Lieven De Strycker
KU Leuven
DRAMCO Research Group
Ghent, Belgium
name.surname@kuleuven.be

Liesbet Van der Perre
KU Leuven
DRAMCO Research Group
Ghent, Belgium
name.surname@kuleuven.be

***Abstract*—An indoor, ultra low power, hybrid signaling localization system is proposed that can position mobile devices with cm-accuracy. The concept is based on the hybrid Time Of Flight principle, which determine distances based on the difference in propagation velocity of mechanical and electromagnetic waves. Recent developments in both the acoustic as well as the radio frequency backscattering domain make it possible to obtain energy neutrality, whilst signal processing can improve the accuracy. A demonstrator proves the principles of this system in a real-life set-up.**

***Index Terms*—Indoor positioning, backscattering, acoustic, low power, WSN's**

I. Introduction

Tracking, indoor navigation and location tagging are some of the applications for indoor localization. In this environment, outdoor positioning services, like GPS, are inaccurate due to obstruction of direct line-of-sight to satellites. Despite intensive research the last couple of years, no low power, cm-accurate solution in indoor positioning has been realized. The majority of the proposed systems make use of time based ranging measurements to obtain the position of a mobile node. The signals used for the localisation measurements can be based on electromagnetic waves, like radio frequency waves or light [1] [2], on mechanical waves, like sound [3] [4], or on a combination of these two, which is our field of interest [5] [6]. The advantage of combining RF and sound is that they have the instantanious character of electromagnetic waves, but errors on signal detection time have less influence on the correct distance calculations due to the slower propagation of mechanical waves.

Two techniques are distinguished in hybrid positioning systems, where either the system or the node itself determine the position. The first one is introduced by the Active Bat Local Positioning System [5]. Fixed beacons on the ceiling receive an ultrasonic signal comming from a mobile emitter. The position is then calculated in a central unit, which triggers the transmission of a new ultrasonic signal by the means of a radio link. The second technique is introduced by the Cricket System [6]. Here the beacons send out an ultrasonic signal together with a radio pulse for synchronization. The mobile device calculates its own position, which ensures its privacy.

Recent studies mainly focus on obtaining high accuracy with as little infrastructure as needed [7] [8]. In the context of Wireless Sensor Networks (WSN), energy is the main contraint. There is little research done on positioning methods that strive for a low power solution, hence research is intensifying [9]. In this paper a system that offers both is proposed. It is based on recent developments in acoustic hardware and on RF backscattering. Current state of the art shows that main purpose of backscattering is communication. With this paper, we exploit the energy advantages of this technology for the purposes of indoor localisation with cm-accuracy.

The next section gives an overview of the system. Section 3 describes the backscattering principle. Next, information on the acoustic side is discussed. Later the measurement results of the proof of concept are presented. And finally, the paper is summarized.

II. Hybrid Acoustic System Overview

A. Distance Measurements

Figure 1 shows the system overview in the first step of the indoor positioning process, namely the distance measurement. It consist of two types of entities, a Transmitter/Receiver (T/R) and an ultra low power mobile node (M) which on their turn use two types of signals to perform hybrid Time Of Flight (TOF) distance measurements. The hybrid TOF consist of measuring the round trip time of an acoustic signal in the first phase (forward direction), and a RF signal in the second one (return trip). The advantage of combining electromagnetic and mechanical waves is that errors introduced by clock drift, conversion delays and multipath interference have less influence on the absolute positioning since the propagation speed of sound is 10^6 lower than the speed of light.

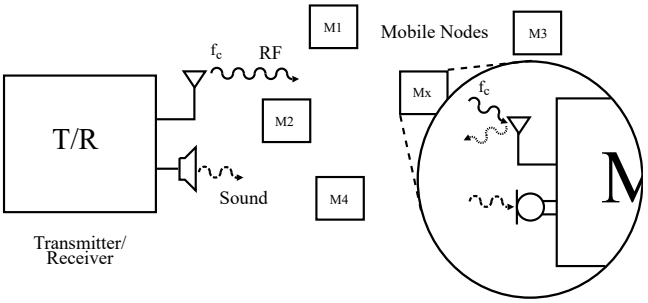

Fig. 1: Distance measurements between transmitter/receiver and mobile nodes.

The T/R initiates the measurements by sending out a continuous RF carrier wave at a desired frequency and a (ultra)sound signal. The audio broadcast triggers the TOF algorithm to start its internal counter (T_1) and is received at the mobile node at a time (T_2) by a a low power MEMS microphone. These signals are amplified and converted to a RF signal in the form of a backscattered signal. This backscattered signal is detected by the T/R as a modulated signal on the initial RF carrier wave (T_3). An overview of the signal transmission and accompanied identifiers can be found in figure 2. The distance Δx can be calculated out of the time difference between T_3 and T_1, and the speed of sound. The term θ (in °C) in equation 1 models the temperature dependency of mechanical waves.

$$\Delta x = 20.0577 \cdot \sqrt{273.15 + \theta} \cdot (T_3 - T_1) \tag{1}$$

There are two main reasons why the sound signal is chosen as the initial signal. First, generating sound that can travel far enough (several meters) costs more energy than receiving it. As we aim for a low-power mobile node, the logical choice is to let the beacons send out the sound signal. Second, the bandwith of most (ultra)sonic transducers is limited. This, in combination with the slow propagation speed, means that only a few beacons can transmit a sound in a limited amount of time. Since the amount of mobile devices in a single room easily can outnumber the amount of T/R, this choice is validated.

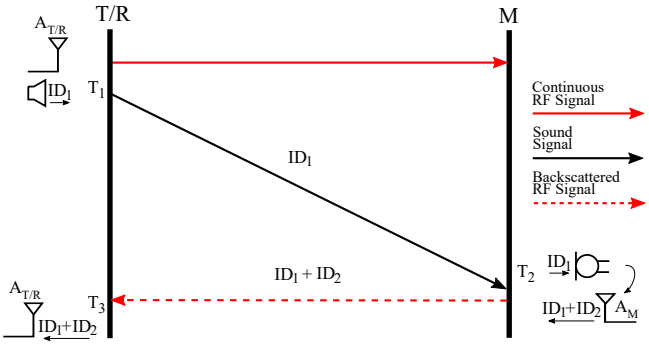

Fig. 2: Timeline of the transmitted and received signals, both on the T/R and mobile nodes.

B. Positioning

The next step is using the known distances to perform indoor positioning. This positioning system is based on the second hybrid positioning technique, in which the system calculates the position of the mobile nodes. For positioning in a 2D environment, the system from figure 1 needs to be elaborated with at least two more T/R's, of which one should act as a central T/R that collects the other distances and perform the trilateration. To perform this classic trilateration, one should know which distance belongs to which mobile node - T/R pair. In other words, identification of the T/R's is necessary. In the literature, there are several ways to identify the beacons. In [8], OFDM is used to create a narrowband orthogonal division-multiplexing signal, which can efficiently utilize the entire available acoustic spectrum. The disadvantage is that the signals still are narrowbanded, which makes them vulnerable to noise and interference. In [10] this is solved by using Frequency Hopping Spread Spectrum (FHSS). Gold codes are used to switch between several frequencies. Next to spectrum spreading of the signals, we can use these codes as a unique identifier of the T/R. Seeing that the audio-signal received on the mobile device is directly converted into a RF signal, it is possible to identify the T/R's in the received RF signals.

The positioning method above is only applicable for the sitation where there is only one mobile node. Adding mobile nodes introduces a new problem: how can we identify not only the T/R but these mobile nodes as well? Passive, mobile node identifiers can be found in RFID. Traditionally, the tag is manually programmed with a specified ID, which is stored in a non-volatile memory. However these memories require large voltages and currents, which in the case of RFID is received throughout wireless power transfer. In [11] and [12], lithographic uncertainty and random dopant fluctuation are used to create a unique, random ID. The tag reads the power-on state of an 128-bit SRAM array and allows reliable identification of IC's without explicit programming. This ID can be added as a backscatter signal after the converted sound signal. In case of noise and interference, OFDM or FHSS in the RF spectrum can be added to the current set up.

III. RF Backscattering for low power communications.

In (hybrid signaling) WSN applications, communication requires a substantial amount of the energy budget. A key concern is how to power these devices, when their size decreases and they grow in number. Instead of researching how to cut down the power, a solution can come from a different angle: how can we communicate completely powerless? In traditional backscatter, used in RFID systems, mobile nodes communicate by causing a change in the field through impedance modulation at the antenna. These changes in the field can be detected at the T/R, hence making it orders of magnitude more energy efficient than conventional radio communication [13].

A key concept in backscattering is the Radar Cross Section [RCS] of the antenna. Fig. 3b shows the equivalent scheme of a simple backscatter system. V_A is the open circuit voltage on the antenna terminals, Z_A the impedance of the antenna itself and Z_T the impedance attached to the antenna terminals. The reflection coefficient of an antenna is given by:

$$\Gamma = \frac{Z_T - Z_A^*}{Z_T + Z_A} \tag{2}$$

It can be seen that the maximum reflection is received when the Z_T equals zero, in other words, when the antenna is shorted.

The RCS of the antenna is defined as:

$$\sigma = \frac{\lambda^2 G_R^2}{4\pi} |1 - \Gamma|^2 \tag{3}$$

With λ the signal wavelength and G_R the receiver antenna gain. Equation 3 shows the ability of the mobile node to reflect the received RF signals in the direction of the T/R. It's observed that maximum RCS can be obtained when the antenna is shorted.
The power density of the electromagnetic waves, received at the mobile node at a distance r is:

$$S = \frac{P_t\, G_t}{4\,\pi\, r^2} \tag{4}$$

With P_t the T/R's transmission power and G_t the T/R's antenna gain (Fig. 3a). With this, the RF power collected by the mobile node can be written as the product of the antenna's effective aperture (A_e) and power density:

$$P_{received} = S\, A_e = \frac{P_t\, G_t}{4\,\pi\, r^2}\, \frac{\lambda^2\, G_r}{4\,\pi} \Big[1 - |\Gamma|^2\Big] \tag{5}$$

Maximum power transfer (when ($|\Gamma| = 0$)) is obtained when the antenna is terminated with the complex conjugated of its own impedance ($Z_T = Z_A^*$). At the same time, optimal power harvesting is received in this state. For thin wire antennas the backscattered power can be written as the product of the RCS and the power density:

$$P_{backscatter} = S\,\sigma = \frac{P_t\, G_t}{4\,\pi\, r^2}\, \frac{\lambda^2\, G_r^2}{4\,\pi} |1 - \Gamma|^2 \tag{6}$$

For optimized detection of the backscattered signal at the T/R, the difference between absorbed or backscattered power in eq. 6 needs to be as large as possible. Crucial in this all is the antenna impedance matching, which is the direct influence of the reflection coefficient.

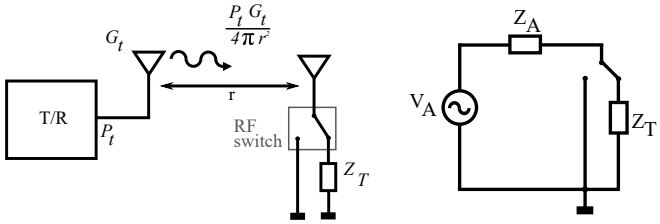

(a) (b)

Fig. 3: Power density received at the mobile node (a) and the equivalent circuit of the backscatter receiver (b).

The backscattering can also be analyzed in the frequency domain.A continuous RF wave $S_{tr}(t)$ is transmitted from the T/R. At the mobile node, the signal $S_{tr}(t)$ is reflected or absorbed depending on the acoustic sequence $B(t)$ received at its microphone. At the T/R this leads to a reflected signal $R(t)$ that consist of two components: the carrier wave $S_{tr}(t)$ and a variated backscattered signal $S_{bt}(t)$

$$R(t) = S_{tr}(t) + \sigma \cdot B(t) \cdot S_{bt}(t) \tag{7}$$

With σ the antenna's radar cross section and $B(t)$ equals 1 when reflecting and 0 when absorbing. [14]
As the backscattering works as a mixing proces between the acoustic signal and the carrier signal, interference between the carrier signal and the weak backscattered reflection is eliminated by sending out a sound signal with a frequency of Δf [15]. The backscattered signal can be rewritten as

$$2\, sin(f_c\, t)\, sin(\Delta f\, t) = cos[(f_c + \Delta f)t] - cos[(fc - \Delta f)t] \tag{8}$$

It appears back at the T/R as an offset of Δf on both sides of the carrier frequency.
As traditional backscatter devices rely on power-hungry components like oscillators and ADCs, the goal in our concept is to eliminate these. The hardware for a backscatter radio consist of a RF switch connected to an antenna (Fig. 3a). The ADG902 and derivates used in [14], [16] and [17] is such a reflective switch. Sending a bitstream on the control-line of this switch changes the impedance of the antenna. Either it matches the antenna and it absorbs the RF signal, or it connects internally to the ground and totally reflects it. The input of this control can be either a level-triggered sound signal or the unique tag ID.
To make optimal use of the spectrum in FDM systems, single sideband reflected signals can be obtained in two ways. The first one is to use a RF-splitter [15]. The splitter copies the original backscatter signal in to two copies on two paths. By performing a square wave multiplication on each path, two double side-banded signals are obtained. By delaying the square wave with a quarter of its period, one of the side bands is a negative copy on one side-band and a positive one on the other. Summing up these two signals gives us an amplification of the original signal on one side and elemination on the other. In [16] a second method is presented that only makes use of passive components, decreasing the overall power. By changing the impedance connected to the antenna, square waves with different voltage levels are obtained. These approximate sine and cosine waves that not only cancel the mirror image but remove the 3th and the 5th harmonics as well.

IV. Acoustic signaling for precise positioning

The sound signal is initiated at the T/R throughout a speaker. The choice of making the T/R as sound source is justified since the generation of sound costs more power, the amount of beacons are limited and these static beacons have access to a fixed power source more easily. At the mobile nodes, MEMS microphones are used for the sound reception. The power consumption of these MEMS microphones is low in comparison to these of typical electret microphones (1.5 mW), from 324 μW in the general purpose InvenSence INMP504 [18] down to 13 μW in the ultra low power Sonion N8AC03 [19]. Yet, this energy saving advantage imposes a larger startup time. Short sound events (< 410 ms), like claps (22 ms), cannot be detected if the microphone needs to be awaked from sleep mode. The acoustic circuit in this case needs to be in an always on state. Another disadvantage of using these microphones with an analog output is the need for strong signal amplification, which increases the power consumption with a factor 6 [20]. Previous measurements

confirmed the omnidirectional behaviour for different types of MEMS microphones at different frequencies [21]. This opens the possibility to use these for broadband acoustic signals, as earlier proposed by the FHSS techniques.

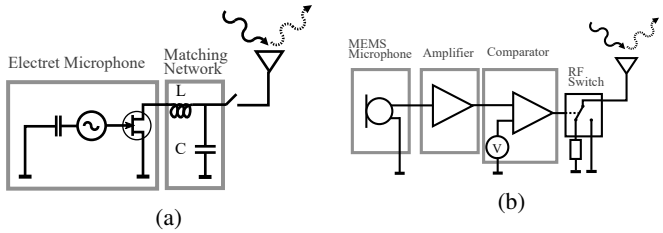

(a) (b)

Fig. 4: Architecture of impedance changed backscattering(a) and the audio signal based backscattering (b).

A. *Hybrid sensing*

There are two ways to combine the microphone with the RF backscattering in a analog way. The first one is proposed by [22] and places an electret condenser microphone between the antenna terminals. Incoming soundwaves change the JFET's gate-source voltage, resulting in a impedance change at the output of the microphone (Z_t). To optimize the backscattering, the input impedance of the JFET is matched to the one of the antenna (Z_A), using an L-C tuning network (Fig. 4a). The disadvantage of this is that for short distances, the JFET gets saturated, resulting in erroneous audio reception. Mismatches introduced by the non-linair variations of the impedance, increase the pathloss and thus degrade the RF-backscattering. In this way, the distance is limited to 2.7m.
This paper exploits another method of acoustic backscattering. Here, the audio signals themselves are used instead of the microphone's impedance. (Fig. 4b) The small audio signals coming out of the MEMS microphones are firstly amplified. Secondly, a comparator compares these augmented signals with an adaptive treshhold level, resulting in a binary signal that drives an RF switch. The RF-switch changes the antenna terminal impedance (Z_T), shorting or matching it to complex conjugated antenna impedance (Z_A^*). This minimizes the mismatch, resulting in optimized RF-backscattering. Saturation of the audio signal isn't a problem in this solution, giving the opportunity to perform distance measurements for short ranges. Another advantage is that we can still switch between several matched impedances, giving the opportunity to cancel out harmonics in future research. However, since additional hardware is added, the power consumption of this setup will be higher.

V. Experiments and validation

A. *Set-up*

Measurements were performed on the first aspect of the hybrid backscattering technique: the initial acoustic sound signal propagation and detection in its simplest form. This means without the usage of a specific sound signal at the transmitter nor were any cross correlation techniques used at the receiver. The amplified and compared, audio signals are directly fed in as input of the RF-back end. This opens the oppurtunity to perform measurements close to the sound source, without the risk on saturation. The main difference with the hardware proposed in figure 4b is that for these measurements, we don't use any form of backscattering. For the RF-communication we used off-the-shelf 433 MHz RF transmitters and receivers at the T/R. The set-up of a T/R and a mobile node can be seen in figure 5. The T/R consist of a "Wonder Gecko EFM32WG-STK3800", a speaker and the 433MHz RF-receiver. At the mobile node, we find the MEMS-microphone, amplifier, comparator and the RF-transmitter. The T/R as well as the Mobile node are powered with a portable 2600 mAh USB power bank.

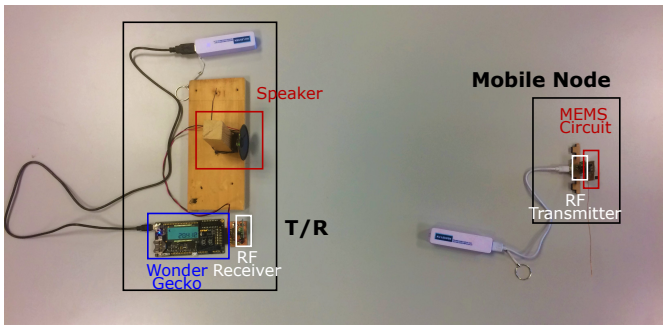

Fig. 5: Set-up for the precision and accuracy measurements. Receiver and transmitter are positioned in the same plain.

The course of the measurements implements the TOF-method. A 4 kHz square wave is generated at the Wonder Gecko and transmitted by the speaker. This sound signal is received by the MEMS microphone and its amplified and compared signal is directly fed into the data input of the RF-transmitter. This 4 kHz RF-signal is instantaniously received at the RF receiver. Time measurements are performed by the Wonder Gecko and the calculated distance is displayed in mm on the LCD-screen. Since we don't use any form of backscattering, the continuous RF signal isn't present, and RF-signals can be detected at the T/R without performing any form of frequency mixing.

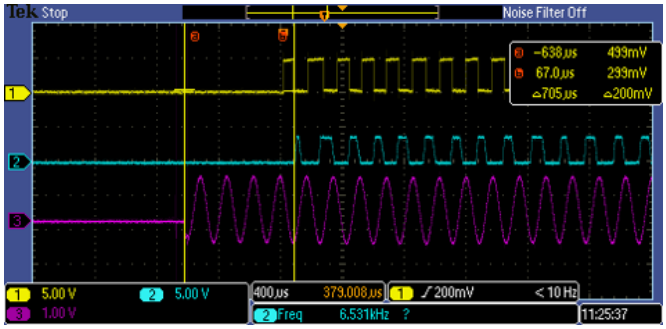

Fig. 6: Fixed delay between received audio signal and transmitted RF signal

The scope image in figure 6 shows the time difference between the received audio signal (in yellow) and the transmitted RF signal (in blue) at a random distance. Measurements at

several distances verify that this is a fixed delay of $60\,\mu$s (≈ 20.4 mm). Adding this delay to the distance measurements equation eleminated the error introduced by the audio to RF conversion.

In the next subsection two types of measurements are performed: the first one tests the accuracy and precision of the system. An image of the setup can be found in figure 5. The mobile node is linearly moved away from the T/R and at specific distances and angles, a large dataset is collected. The second set of measurements tests the system boundaries at different angles. Fig. 7 depicts the set-up. Distance data is collected at concentric half circles around the speaker with a spacing of 20cm. The speaker is directed towards the 0° angle and the mobile node is moved around the half circles in steps of 15°. The microphone at the mobile node is always directed towards the speaker. However, this isn't required, as previous measurements show the omnidirectional charachter of the MEMS microphones.

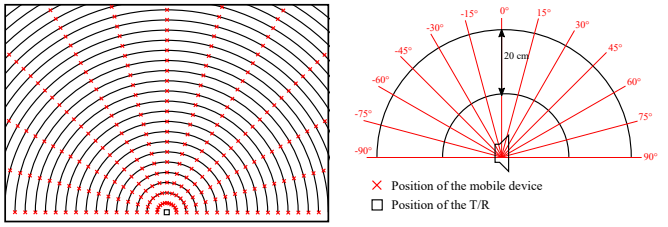

Fig. 7: Set-up for system boundaries measurements in the audible domain.

TABLE I: Precision and accuracy measurements at 1 m.

Angle (°)	Mean (mm)	Median (mm)	σ (mm)	Min. (mm)	Max. (mm)	P95 (mm)	P99 (mm)	Ref. (mm)
0	966,63	965	19,54257	916	1039	1026,5	1037	1002
45	953,28	954	11,52869	929	1027	968	1001	1002
90	1047,32	1073	36,3365	990	1083	1079	1082	1002
135	1026,08	1060,5	40,70606	973	1074	1068	1072,5	1002
180	995,6	986	26,71057	963	1068	1065	1068	1002

B. Ranging accuracy analysis

Tables I and II displays the results of the precision and accuracy measurements for two distances at several angles. For every angle at these distances, 100 samples were collected. The reference distances were obtained with a Bosch GLM30 laser rangefinder which has an accuracy of ± 2 mm. To get an indication of the precision, we compare the mean of the measurements with the refecerce distance. For the smaller distance, the precision is less than 50 mm at each angle, and this with a standard deviation of around 20 mm at small angles, and 40 mm for the larger ones. The P95 and P99 values show that the outliers are limited. At the larger distance, we note that at certain angles, the system doesn't receive the sound signal anymore. Yet at the remaining angles, we still see that the difference between the mean and the reference value is smaller than 60 mm with a standard deviation of 40 mm. Again, the P95 and P99 values show that the outliers are rather small.
When we compare the mean and the median with each other, we note that the difference between these two is rather large. This is explained through inspection at the histogram in such a scenario (figure 8). We notice that this isn't the aspected normal distribution, in fact there are two peaks, seperated from each other by about 80 mm. Since the interrupts generated at the RF-input of the Wonder Gecko is positive edge triggered, missing the initial pulse of the 4 kHz square wave equals $\frac{330\,m/s}{4000\,Hz} = 82.5$ mm and thus correspondends with this 80 mm. Parameters like unsignificant signal amplification at both transmitter as receiver and, microphone and speaker response time can cause these late detections. False detections caused by sound signals comming from other surrounding sources decreases the precision and accuracy. In our research these signals didn't occur due to the silent surroundings in which the measurements took place. In future research these erroneous detections can be eliminated by using cross correlation at the T/R side. Since we know which acoustic signal is transmitted and that same signal is received at the RF side, improvements on false detections and accuracy can be obtained.

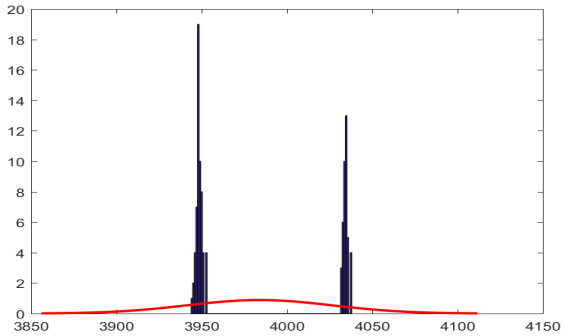

Fig. 8: Histogram of the measured distances at 4m at an angle of 180 degrees.

The second type of measurements show the system boundaries. Every 20 centimeters, at angles going from 0° to 180° we took 10 samples. To validate the obtained distances, we took the absolute value of the difference between the actual distance and the mean value of the conforming data set. With this error, we can generate a heat map in which the distance boundaries are given for several angles (Figure 9). The error and the distances in this figure are all in mm. The dark red collor on this heat map tells us that the system performs well for distances smaller than 2 m. The error in this case is smaller than 50 mm, which is confirmed in earlier analysis. For larger distances, the angle between the sound source and receiver becomes more and more important. Perpendicularly on the speaker distances up to 9 meters are obtained. When the mobile node is moved towards the 90° angle, this error increases and the maximum distance is cut back to 2.6 m. Note that the heat map itself is determined by the speaker and microphone directivity, signal amplification at both sides, room response, speaker frequency response, etc. but it gives an impression of how the system reacts with fixed parameters.

TABLE II: Precision and accuracy measurements at 4m.

Angle (°)	Mean (mm)	Median (mm)	σ (mm)	Min. (mm)	Max. (mm)	P95 (mm)	P99 (mm)	Ref. (mm)
0	3981,1	3980	7,967738	3976	4059	3982	4021	4001
45	4059,86	4064	19,2007	3982	4070	4068	4070	4001
90	0	0	0	0	0	0	0	4001
135	0	0	0	0	0	0	0	4001
180	3983,86	3950	42,59701	3944	4038	4036	4038	4001

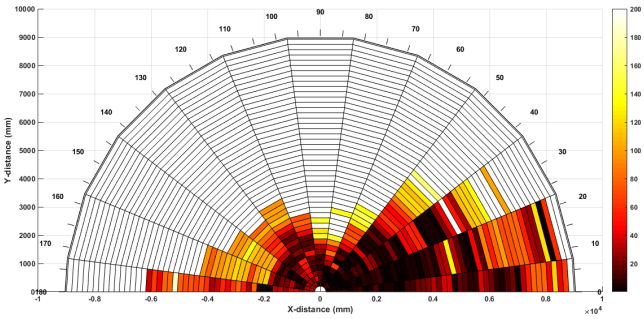

Fig. 9: Heat map of the boundary measurements in the audible spectrum.

In all measurements, we noted that there are several cases in which the calculated distance is smaller than the actual distance. Does this mean that the actual distance is the smallest measured? In equation 1, we stated the temperature dependancy of the speed of sound. In the current set-up, this is a fixed value of 340 m/s (the speed of sound at 14° C), meaning that if the temperature rises to 21° C the speed of sound rises with 4 m/s resulting in 1.47% decrease of distance. For a distance of 5 m, this is the same as 73.5 mm error, which in our case is sometimes equalized by the 82.5 mm introduced by the skipped initial sound pulse. Adding a temperature sensor and inserting this information as a variable in the measurements can counteract this problem.

VI. Conclusion

In this work we introduced an ultra low-power solution for cm-accurate distance and positioning purposes. This system concept uses hybrid signaling throughout MEMS microphones and RF backscattering. Solutions for key concepts like identification of the beacons and mobile nodes are proposed as well as an overview of the current backscatter state-of-the art is given. Measurements on the acoustic side of this system show promising results of cm-accuracy within 2 m radius around the speaker, and maintaining this accuracy for distance up to 9.6 m in the dominant directions. Improvements are proposed in the form of matched filtering or adding aditional hardware to overcome environmental dependant parameters.
Future work will focus on the application of the proposed improvements and implementing the backscatter as the RF-back end in this promising system.

References

[1] H. Liu, H. Darabi, P. Banerjee, and J. Liu, "Survey of wireless indoor positioning techniques and systems," *IEEE Trans. Syst. Man Cybern. Syst. Part C: Applications and Reviews*, vol. 37, no. 6, pp. 1067–1080, November 2007.

[2] S. De Lausnay, L. De Strycker, J. P. Goemaere, N. Stevens, and B. Nauwelaers, "Optical cdma codes for an indoor localization system using vlc," *International Workshop in Optical Wireless Communications*, pp. 50–54, January 2014.

[3] I. Rishabh, D. Kimber, and J. Adcock, "Indoor localization using controlled ambient sounds," *International Conference on Indoor Positioning and Indoor Navigation*, November 2012.

[4] O. Khyam, S. S. Ge, X. Li, and M. R. Pickering, "Highly accurate time-of-flight measurement technique based on phase-correlation for ultrasonic ranging," *Sensors*, vol. 17, no. 2, pp. 434–443, January 2017.

[5] M. Addlesee, R. Curwen, S. Hodges, J. Newman, P. Steggles, A. Ward, and A. Hopper, "Implementing a sentient computing system," *Computer*, vol. 34, no. 8, pp. 50–56, 2001.

[6] N. B. Priyantha, "The cricket indoor location system," Ph.D. dissertation, Computer Science and Engineering, MIT, 2005.

[7] C. Medina, C. J. Segura, and A. De la Torre, "Ultrasound indoor positioning system based on a low-power wireless sensor network providing sub-centimeter accuracy," *Sensors*, vol. 13, pp. 3501–3526, March 2013.

[8] O. Khyam, J. Alam, A. J. Lambert, A. M. Garratt, and M. R. Pickering, "High-precision ofdm-based multiple ultrasonic transducer positioning using a robust optimization approach," *Sensors*, vol. 16, no. 13, pp. 5325–5336, July 2016.

[9] Y. Zhao and J. R. Smith, "A battery-free rfid-based indoor acoustic localization platform," *IEEE International conference on RFID*, pp. 110–117, 2013.

[10] L. Segers, J. Tiete, A. Braeken, and A. Touhafi, "Ultrasonic multiple-access ranging system using spread spectrum and mems technology for indoor localization," *Sensors*, vol. 17, no. 2, pp. 434–443, February 2014.

[11] D. Yeager, F. Zhang, A. Zarrasvand, N. T. George, T. Daniel, and B. P. Otis, "A 9 ua, addressable gen2 sensor tag for biosignal acquisition," *IEEE Journal Of Solid-State Circuits*, vol. 45, no. 10, pp. 2198–2209, October 2010.

[12] Y. Su, J. Holleman, and B. P. Otis, "A digital 1.6 pj/bit chip identification circuit using process variations," *IEEE Journal Of Solid-State Circuits*, vol. 43, no. 1, pp. 69–77, January 2008.

[13] M. Buettner, "Backscatter protocols and energy-efficient computing for rf-powered devices," Ph.D. dissertation, University of Washington, 2012.

[14] A. Varshney, O. Harms, C. Perez-Penichet, C. Rohner, F. Hermans, and T. Voigt, "Lorea: A backscatter architecture that achieves a long communication range," *Sensys*, vol. 15, November 2017.

[15] P. Zhang, D. Bharadia, K. Joshi, and K. Sachin, "Hitchhike: Practical backscatter using commodity wifi," *Sensys*, vol. 14, November 2016.

[16] V. Talla, M. Hessar, B. Kellogg, A. Najafi, J. R. Smith, and S. Gollakota, "Lora backscatter: Enabling the vision of ubiquitous connectivity," *ACM on Interactive, Mobile, Wearable and Ubiquitous Technologies*, vol. 1, no. 3, pp. 105:00–105:24, September 2017.

[17] V. Talla, B. Kellogg, S. Gollakota, and J. R. Smith, "Battery-free cellphone," *ACM on Interactive, Mobile, Wearable and Ubiquitous Technologies*, vol. 1, no. 2, pp. 2500–2520, June 2017.

[18] *Ultra-Low Noise Microphone with Bottom Port and Analog Output*, Invensense, 2014, rev. 1.1.

[19] *Data Sheet microphone*, Sonion, 8 2014, rev. 1.

[20] B. Thoen, G. Ottoy, and L. De Strycker, "An ultra-low-power omnidirectional mems microphone array for wireless acoustic sensors," *Sensors*, October 2017.

[21] B. Cox, B. Thoen, V. Rijmen, L. De Strycker, and V. der Perre, "Directivity assessment of mems microphones in microphone array applications," *Symposium on Information Theory and Signal Processing in the Benelux*, pp. 41–48, May 2017.

[22] V. Talla and J. R. Smith, "Hybrid analog-digital backscatter: A new approach for battery-free sensing," *2013 IEEE International Conference on RFID*, pp. 74–81, April 2013.